Anti-Plane Moving Polarization Saturation Crack in Ferroelectric Solids

Hao-sen Chen[2], Dai-ning Fang[1]

1 LTCS and College of Engineering, Peking University, Beijing, 100871, China
2Department of Engineering Mechanics, Tsinghua University, Beijing 100084, China
* Corresponding author: chenhs09@mails.tsinghua.edu.cn

Abstract
A moving polarization saturation (PS) model is proposed to study the anti-plane Yoffe-type crack with constant velocity in ferroelectric materials. Based on the extended Stroh formalism, the model is solved using complex function method. The closed-form expressions for the electroelastic fields are obtained in a concise way. Results are shown to converge to known solutions for static PS model and the moving linear piezoelectric model.
Keywords Moving polarization saturation model; Ferroelectric materials; anti-plane.

1 Introduction

Ferroelectric materials always endure dynamic loads, such as mechanical impact or pulse-like electric loading in application [1]. Since their instinct low fracture toughness, the reliability concerns and optimal design of smart devices using ferroelectrics call for a better understanding of the fracture behavior. Compared with the well developed static piezoelectric fracture mechanics, few investigations on the dynamic fracture mechanics of piezoelectric and ferroelectric materials have been reported.

The crack propagation problem is always the popular point of study among the theoretical dynamic fracture mechanics. Freund [2] classified the problems of crack propagation into three classes (1) The first type is the steady state crack growth. Chen and Yu [3] studied the anti-plane moving crack problem in piezoelectric materials. They found that the intensity factors are independent of the velocity of the crack. Soh et al. [4] researched the generalized plane problem of a finite Griffith crack moving with constant velocity in an anisotropic piezoelectric material. (2) The second type is self-similar crack growth. (3) The third type is the crack growth due to time-independent or time-dependent loading. In this case, Li and Mataga [5, 6] obtained the transient closed-form solutions for dynamic stress and electric displacement intensities and dynamic energy release rate of a propagating crack in homogeneous hexagonal piezoelectric materials dynamic anti-plane point loading. To et al. [7] studied propagation of a mode-III interfacial conductive crack along a conductive interface between two piezoelectric materials. Chen et al. [8] researched the problem of dynamic interfacial crack propagation in elastic–piezoelectric bi-materials subjected to uniformly distributed dynamic anti-plane loadings on crack faces.

All the aforementioned studies on the problems of crack propagation are mainly about the linear dynamic fracture mechanics. However, when the electrical load is not weak, ferroelectric materials exhibit strong electrical nonlinearity, Gao et al. [9] proposed a strip polar saturation (PS) model of electrical yielding. It is convenient to propose some simplified models or approximate analyses. Shen et al. [10] developed a strip electric saturation and mechanical yielding model for a mode III interfacial crack of Yoffe type between ferroelectric-plastic bi-materials.

In this paper, the static PS model is extended to the moving PS model for studying the anti-plane crack propagation problem of ferroelectric materials. The plan of the rest of the paper is

as follows. Section 2 introduces the governing equations and the boundary conditions. Section 3 proposes the moving PS model and solves the problem using the complex function method. And the explicit expressions of the electroelastic fields are obtained. Section 4 discusses the anti-plane case. Finally, Section 5 gives the conclusions.

2 Statement of the problem

Consider an infinite ferroelectric medium containing a Yoffe-type crack of fixed length 2*a*,which moves through an otherwise unbounded ferroelectric materials at speed *v*, with the crack opening at the leading crack tip and closing at the trailing crack speed. The ferroelectric solids are considered as a class of mechanically brittle and electrically ductile solids. The electrical polarization is assumed to be saturated only in a line segment in front of the crack. And the medium is subjected to remote uniform electro-mechanical loads as shown in Fig.1.

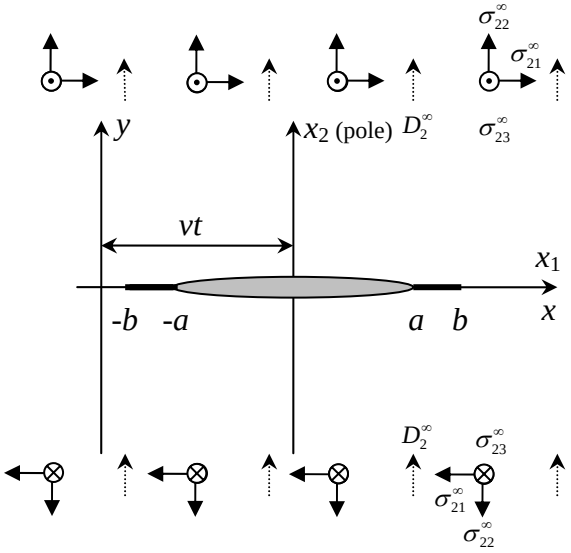

Fig.1. Schematic representation of the moving PS model

2.1 Basic equations

Our earlier work [4] has proposed the governing equations of the piezoelectric material and given the solutions using the Stroh formalism method in details. For the reason of a self-contained presentation, the basic equations and the solution method are also summarized as follows.

In a rectangular coordinate system x_i (i =1, 2, 3), the momentum balance equations and quasi static Maxwell equation for quasi-electrostatic piezoelectricity are as follows

$$\sigma_{ij,j} = \rho\, \partial^2 u_i / \partial t^2 , \quad D_{i,i} = 0 \tag{1}$$

where ρ is the density of the material, u_i, σ_{ij} and D_i are the elastic displacements, stresses, and electric displacements, respectively, and a subscript comma denotes partial differentiation with respect to one of the coordinates x_i. The constitutive relations are

$$\sigma_{ij} = c_{ijkl} u_{k,l} + e_{ijk} \phi_{,k} , D_i = e_{ikl} u_{k,l} - \varepsilon_{ik} \phi_{,k} \tag{2}$$

where ϕ is the electric potential, the electric fields E_i are related to ϕ as $E_i = -\phi_{,i}$, c_{ijkl}, e_{kij} and ε_{ij} are the elastic stiffness, piezoelectric and dielectric constants, respectively.

For a two-dimensional problem, all the variables are independent of x_3, Eqs. (1) and (2) can be expressed in the following compact form:

$$\boldsymbol{t}_{1,1} + \boldsymbol{t}_{2,2} = \rho \boldsymbol{g} \ddot{\boldsymbol{U}} \tag{3}$$

$$\boldsymbol{t}_1 = \boldsymbol{Q}\boldsymbol{U}_{,1} + \boldsymbol{R}\boldsymbol{U}_{,2}, \quad \boldsymbol{t}_2 = \boldsymbol{R}^{\mathrm{T}}\boldsymbol{U}_{,1} + \boldsymbol{T}\boldsymbol{U}_{,2} \tag{4}$$

where $\boldsymbol{U} = [u_1, u_2, u_3, \phi]^{\mathrm{T}}$, $\boldsymbol{t}_\beta = [\sigma_{\beta 1}, \sigma_{\beta 2}, \sigma_{\beta 3}, D_\beta]^{\mathrm{T}}$ (β =1,2), and $\boldsymbol{g} = \mathrm{diag}[1,\ 1,\ 1,\ 0]$. The matrices $\boldsymbol{Q}$, $\boldsymbol{R}$ and $\boldsymbol{T}$ are related to the material constants by

$$\boldsymbol{Q} = \begin{bmatrix} c_{i1k1} & e_{1i1} \\ e_{1k1}^{\mathrm{T}} & -\varepsilon_{11} \end{bmatrix}, \quad \boldsymbol{R} = \begin{bmatrix} c_{i1k2} & e_{1i2} \\ e_{2k1}^{\mathrm{T}} & -\varepsilon_{12} \end{bmatrix}, \quad \boldsymbol{T} = \begin{bmatrix} c_{i2k2} & e_{2i2} \\ e_{2k2}^{\mathrm{T}} & -\varepsilon_{22} \end{bmatrix} \tag{5}$$

Substituting Eq. (4) into Eq. (3) leads to

$$\boldsymbol{Q}\boldsymbol{U}_{,11} + \left(\boldsymbol{R} + \boldsymbol{R}^{\mathrm{T}}\right)\boldsymbol{U}_{,12} + \boldsymbol{T}\boldsymbol{U}_{,22} = \rho \boldsymbol{g} \partial^2 \boldsymbol{U} / \partial t^2 \tag{6}$$

2.2 Yoffe-type crack

As shown in Fig.1. (x, y, z) is a moving coordinate system fixed on the crack with the center as its origin. It has the relation with the fixed coordinate system (x_1, x_2, x_3) as follows

$$x = x_1 - vt, \quad y = x_2, \quad z = x_3 \tag{7}$$

Then

$$\frac{\partial}{\partial t} = -v\frac{\partial}{\partial x} \tag{8}$$

Thus, Eq. (6) can be written as

$$\left(\boldsymbol{Q} - \rho v^2 \boldsymbol{g}\right)\boldsymbol{U}_{,xx} + \left(\boldsymbol{R} + \boldsymbol{R}^{\mathrm{T}}\right)\boldsymbol{U}_{,xy} + \boldsymbol{T}\boldsymbol{U}_{,yy} = \boldsymbol{0} \tag{9}$$

Eq. (9) is the governing differential equation for the steady-state electroelastic fields. Note that the structure is identical to that of the static case when ($\boldsymbol{Q} - \rho v^2 \boldsymbol{g}$) is identified with $\boldsymbol{Q}$.

2.3 Boundary conditions

The medium is subjected to remote uniform electro-mechanical loads given by $\boldsymbol{t}_2^{\infty} = [\sigma_{21}^{\infty}, \sigma_{22}^{\infty}, \sigma_{23}^{\infty}, D_2^{\infty}]^{\mathrm{T}}$. The crack surfaces are traction-free and charge-free, with electrical yielding along strip $a \leqslant |x| \leqslant b$.

The full set of boundary conditions for the moving PS model considered in this paper can be summarized as

$$\boldsymbol{t}^{+} = \boldsymbol{t}^{-} = -\boldsymbol{t}_2^{\infty}, \qquad \text{at} \quad |x| < a \tag{10a}$$

$$u_i^{+} = u_i^{-},\ i=1,\ 2,\ 3, \quad D_2^{+} = D_2^{-} = -D_2^{\infty} + D_s, \qquad \text{at} \quad a \le |x| \le b \tag{10b}$$

$$\boldsymbol{t} = 0 \qquad \text{at} \quad y \to \infty \tag{10c}$$

where D_s is the electrical saturation limit.

3 Solution of the problem

3.1 Full field solution

Adopting Stroh formalism for anisotropic elasticity, a general solution to Eq. (9) can be sought in the form

$$\boldsymbol{U} = \boldsymbol{a} f\left(z\right), \quad z = x + \mu y \tag{11}$$

where μ and $\boldsymbol{a}$ are a constant and a constant vector respectively; and $f(z)$ is an arbitrary function of variable z subject to the twice-differentiable requirement. Substitution of Eq. (11) into Eq. (9) results in

$$\left[\mathbf{Q} - \rho v^2 \mathbf{g} + \mu\left(\mathbf{R} + \mathbf{R}^{\mathrm{T}}\right) + \mu^2 \mathbf{T}\right]\boldsymbol{a} = 0 \tag{12}$$

This is a nonlinear eigenvalue problem. A nontrivial solution of $\boldsymbol{a}$ requires that the determinant of its coefficient matrix must be zero, i.e.,

$$\det\left[\mathbf{Q} - \rho v^2 \mathbf{g} + \mu\left(\mathbf{R} + \mathbf{R}^{\mathrm{T}}\right) + \mu^2 \mathbf{T}\right] = 0 \tag{13}$$

This is a polynomial of degree 8 for μ. If μ_α (α = 1, 2, 3, 4) are assumed to be the four distinct roots with positive imaginary parts, and $\boldsymbol{a}_\alpha$ are the associated eigenvectors, the general solution can then be expressed as

$$\boldsymbol{U} = 2\Re\sum_{\alpha=1}^{4} \boldsymbol{a}_\alpha f_\alpha\left(z_\alpha\right) \tag{14}$$

where $\Re$ denotes the real part and $z_\alpha = x + \mu_\alpha y$.

Substituting Eq. (14) into Eq. (4) and by using Eq. (3), the stress and electric displacement vectors can be expressed as

$$\boldsymbol{t}_1 = -\boldsymbol{\Phi}_{,y} + \rho v^2 \boldsymbol{g} \boldsymbol{U}_{,x}, \quad \boldsymbol{t}_2 = \boldsymbol{\Phi}_{,x} \tag{15}$$

in which

$$\boldsymbol{\Phi} = 2\Re\sum_{\alpha=1}^{4} \boldsymbol{b}_\alpha f_\alpha\left(z_\alpha\right) \tag{16}$$

where $\boldsymbol{\Phi} = [\phi_1, \phi_2, \phi_3, \phi_4]^{\mathrm{T}}$ is called the generalized stress function vector, and $\boldsymbol{b}_\alpha$ can be determined from $\boldsymbol{a}_\alpha$ by the following relation:

$$\boldsymbol{b}_\alpha = \left(\boldsymbol{R}^{\mathrm{T}} + \mu_\alpha \boldsymbol{T}\right)\boldsymbol{a}_\alpha = -\left[\left(\boldsymbol{Q} - \rho v^2 \boldsymbol{g}\right)\mu_\alpha^{-1} + \boldsymbol{R}\right]\boldsymbol{a}_\alpha \tag{17}$$

Introducing two 4×4 matrices, i.e.,

$$\boldsymbol{A} = \left[\boldsymbol{a}_1, \boldsymbol{a}_2, \boldsymbol{a}_3, \boldsymbol{a}_4\right], \quad \boldsymbol{B} = \left[\boldsymbol{b}_1, \boldsymbol{b}_2, \boldsymbol{b}_3, \boldsymbol{b}_4\right] \tag{18}$$

and a function vector, i.e.,

$$\boldsymbol{f}(z_\alpha)=\left[f_1(z_1),\, f_2(z_2),\, f_3(z_3),\, f_4(z_4)\right]^{\mathrm{T}} \tag{19}$$

Then Eqs. (14) and (16) can be rewritten as

$$\boldsymbol{U}=2\Re\left[\boldsymbol{A}\boldsymbol{f}\left(z_\alpha\right)\right],\quad \boldsymbol{\Phi}=2\Re\left[\boldsymbol{B}\boldsymbol{f}\left(z_\alpha\right)\right] \tag{20}$$

Eqs. (15) and (20) together with the relations given by Eq. (17) are the main results of this section. In these expressions, the only unknown is the function vector $\boldsymbol{f}(z_\alpha)$. The appropriate form of $\boldsymbol{f}(z_\alpha)$ depends on the boundary conditions.

In order to obtain the function vector $\boldsymbol{f}(z_\alpha)$, following the same procedure [11, 12], the continuity of $\boldsymbol{t}$(x) on the whole real axis is

$$\boldsymbol{B}\boldsymbol{f}^{'+}(x)+\overline{\boldsymbol{B}}\,\overline{\boldsymbol{f}}^{'-}(x)=\boldsymbol{B}\boldsymbol{f}^{'-}(x)+\overline{\boldsymbol{B}}\,\overline{\boldsymbol{f}}^{'+}(x),\qquad -\infty<x<+\infty \tag{21}$$

A new complex function vector $\boldsymbol{h}(z)$ is defined as

$$\boldsymbol{h}(z)=\boldsymbol{B}\boldsymbol{f}^{'}(z)=\overline{\boldsymbol{B}}\,\overline{\boldsymbol{f}}^{'}(z) \tag{22}$$

And it should satisfy the boundary conditions (10) along the crack faces

$$\boldsymbol{h}^{+}(x)+\boldsymbol{h}^{-}(x)=-\boldsymbol{t}_2^{\infty},\quad |x|<a \tag{23}$$

We also have

$$i\boldsymbol{\delta}^{'}(x)=\boldsymbol{H}\boldsymbol{B}\boldsymbol{f}^{'+}(x)-\boldsymbol{H}\boldsymbol{B}\boldsymbol{f}^{'-}(x) \tag{24}$$

where $\boldsymbol{\delta}^{'}(x)=\{u_1^{+}-u_1^{-},u_2^{+}-u_2^{-},u_3^{+}-u_3^{-},\phi^{+}-\phi^{-}\}$ is the generalized opening displacement, In addition, other two matrices are defined by

$$\boldsymbol{H}=2\Re[i\boldsymbol{A}\boldsymbol{B}^{-1}],\quad \boldsymbol{H}^{-1}=\boldsymbol{\Lambda} \tag{25}$$

Introduce a new complex function vector

$$\boldsymbol{g}(z)=\boldsymbol{H}\boldsymbol{B}\boldsymbol{f}^{'}(z) \tag{26a}$$

$$\boldsymbol{f}^{'}(z)=\boldsymbol{B}^{-1}\boldsymbol{H}^{-1}\boldsymbol{g}(z) \tag{26b}$$

And the next task is to determine the unknown complex function vector $\boldsymbol{g}(z)$. The $g_1(z)$, $g_2(z)$ and $g_3(z)$ are holomorphic functions in whole z plane with a cut ($-a$, a). $g_4(z)$ is holomorphic in whole z plane with a cut ($-c$, c).

Thus, using the Eqs. (23) and (10), we have the following equations

$$\Lambda_{1j}(g_j^{+}(x)+g_j^{-}(x))+\Lambda_{44}(g_4^{+}(x)+g_4^{-}(x))=-\sigma_{21}^{\infty},\qquad |x|<a \tag{27a}$$

$$\Lambda_{2j}(g_j^{+}(x)+g_j^{-}(x))+\Lambda_{44}(g_4^{+}(x)+g_4^{-}(x))=-\sigma_{22}^{\infty},\qquad |x|<a \tag{27b}$$

$$\Lambda_{3j}(g_j^{+}(x)+g_j^{-}(x))+\Lambda_{44}(g_4^{+}(x)+g_4^{-}(x))=-\sigma_{23}^{\infty},\qquad |x|<a \tag{27c}$$

$$\Lambda_{4j}(g_j^{+}(x)+g_j^{-}(x))+\Lambda_{44}(g_4^{+}(x)+g_4^{-}(x))=-D_2^{\infty},\qquad |x|<a \tag{27d}$$

$$\Lambda_{4j}(g_j^+(x)+g_j^-(x))+\Lambda_{44}(g_4^+(x)+g_4^-(x))=-D_2^\infty+D_s,\quad a\le|x|\le b \tag{27e}$$

where the Einstein summation convention for repeated indices is adopted, and j ranges from 1 to 3.

Solving the Eqs. (27a), (27b), (27c) and (27d) gives the following equation

$$\Lambda_{ij}^*(g_j^+(x)+g_j^-(x))=-t_{2i}^{\infty *},\quad |x|<a \tag{28}$$

where $\Lambda_{mj}^*=\Lambda_{mj}-\Lambda_{m4}\Lambda_{4j}/\Lambda_{44}$, $t_{2j}^{\infty *}=t_{2j}^\infty-t_{24}^\infty\Lambda_{j4}/\Lambda_{44}$, m, j=1, 2, 3.

Thus, we can obtain [12]

$$\Lambda^*\boldsymbol{g}^*(z)=\boldsymbol{t}_2^{\infty *}f_0'(z),\quad \boldsymbol{g}^*(z)=(\Lambda^*)^{-1}\boldsymbol{t}_2^{\infty *}f_0'(z),\qquad |x|<a \tag{29}$$

where

$$\boldsymbol{\Lambda}^*=[\Lambda_{mj}^*]_{3\times 3} \tag{30a}$$

$$\boldsymbol{g}^*=[g_1(z),g_2(z),g_3(z)]^T \tag{30b}$$

$$\boldsymbol{t}_2^{\infty *}=[t_{21}^{\infty *},t_{22}^{\infty *},t_{23}^{\infty *}]^T \tag{30c}$$

$$f_0'(z)=\frac{1}{2}\left(\frac{z}{\sqrt{z^2-a^2}}-1\right) \tag{30d}$$

Solving Eqs. (27d) and (27e), we have

$$g_4(z)=\{-\Lambda_{4j}g_j(z)+t_{24}^\infty f_b'(z)\}/\Lambda_{44}+D_s g_0(z)/\Lambda_{44} \tag{31}$$

where $g_0(z)$ has the same property as the function $g_4(z)$, which is holomorphic in whole z plane with a cut ($-c$, c).

$$f_b'(z)=\frac{1}{2}\left(\frac{z}{\sqrt{z^2-b^2}}-1\right) \tag{32a}$$

$$g_0(z)=\frac{1}{\pi}\left\{\frac{\pi}{2}-\frac{1}{2i}\log\frac{\frac{z}{a}\frac{\sqrt{b^2-a^2}}{\sqrt{z^2-b^2}}+i}{\frac{z}{a}\frac{\sqrt{b^2-a^2}}{\sqrt{z^2-b^2}}-i}-\frac{z}{\sqrt{z^2-b^2}}\arccos\left(\frac{a}{b}\right)\right\} \tag{32b}$$

Furthermore, $g_0(z)$ has the following property on the crack faces

$$g_0^+(x)+g_0^-(x)=0,\quad |x|<a \tag{33a}$$

$$g_0^+(x)+g_0^-(x)=1,\quad a\le|x|\le b \tag{33b}$$

Wang [12] gave the method to calculate the function $\log\frac{z+i}{z-i}$.

$$\log\frac{z+i}{z-i}=\log\frac{r_2}{r_1}+i(\theta_2-\theta_1) \tag{34}$$

where r_1 and r_2 are the modulus of the complex variables $z+i$ and $z-i$ respectively. θ_1 and θ_2 are the inclined angles of the complex variables $z+i$ and $z-i$ with respect to the negative imaginary axis. From Eqs. (29) and (31), the unknown complex function vector $\boldsymbol{g}(z)$ has been obtained. Then substituting the result into Eq.(26b), we can derive the unknown function vector $\boldsymbol{f}'(z)$, which provides the full-field solutions of the problem using Eq. (15).

3.2 Electric saturation zone size

From Eq. (15), we obtain the electric displacement ahead of the crack tip

$$\begin{aligned} D_2 &= \Lambda_{4j}(g_j^+(x)+g_j^-(x))+\Lambda_{44}(g_4^+(x)+g_4^-(x)) \\ &= 2T_4 f_b'(x)+D_s(g_0^+(x)+g_0^-(x)) \\ &= (D_2^\infty-\frac{2}{\pi}D_s\arccos(\frac{a}{b}))\frac{x}{\sqrt{x^2-b^2}}-D_2^\infty+D_s\frac{2}{\pi}\left\{\frac{\pi}{2}-\frac{1}{2i}\log\frac{\frac{x}{a}\frac{\sqrt{b^2-a^2}}{\sqrt{x^2-b^2}}+i}{\frac{x}{a}\frac{\sqrt{b^2-a^2}}{\sqrt{x^2-b^2}}-i}\right\} \end{aligned} \tag{35}$$

In order to ensure the non-singularity of the electric displacement at $|x|=b$, Eq. (35) only has a solution if the coefficient of the singular term $\frac{x}{\sqrt{x^2-b^2}}$ vanishes. The following equations must be satisfied

$$\frac{a}{b}=\cos(\frac{\pi}{2}\frac{D_2^\infty}{D_s}) \tag{36}$$

From the above equation, we can calculate the size of the electric saturation zone

$$r=b-a=a\sec(\frac{\pi}{2}\frac{D_2^\infty}{D_s})-a \tag{37}$$

Under small-scale yielding conditions, r<<a, Eq. (37) can be approximately reduced to $r=\frac{a}{2}(\frac{\pi}{2}\frac{D_2^\infty}{D_s})^2$.

3.3 Electroelastic fields near the crack tip

From Eqs. (15) and (20), the stresses and electric displacements can be obtained

$$\boldsymbol{t}_1 = 2\Re\left[\sum_{\alpha=1}^{4}(\rho v^2 \boldsymbol{g}_\alpha \boldsymbol{a}_\alpha f_\alpha^{'}(z_\alpha) - \mu_\alpha \boldsymbol{b}_\alpha f_\alpha^{'}(z_\alpha))\right] \tag{38}$$

$$\boldsymbol{t}_2 = 2\Re\left[\sum_{\alpha=1}^{4}\boldsymbol{b}_\alpha f_\alpha^{'}(z_\alpha)\right] \tag{39}$$

It is obvious that the distributions of the electroelastic fields near the crack tip are of great interest to us. By introducing a polar coordinate system (r, θ) with the origin at the crack right tip, we have

$$z_\alpha - a = r(\cos\theta + \mu_\alpha \sin\theta) \tag{40}$$

When r is small compared to the half-length a of the crack, $z_\alpha \approx a$. Eqs. (30d), (32d) and (34b) can be expressed as

$$f_0^{'}(z_\alpha) = \frac{1}{2}\left(\sqrt{\frac{a}{2r}}\frac{1}{\sqrt{\cos\theta + \mu_\alpha \sin\theta}} - 1\right) \tag{41a}$$

$$f_b^{'}(z) = \frac{1}{2}\left(\frac{1}{i}\frac{a}{\sqrt{b^2 - a^2}} - 1\right) \tag{41b}$$

$$\log\frac{z+i}{z-i} = i(\pi - 2\tan^{-1} a) \tag{41c}$$

From Eq. (39), the stress in front of the crack tip on the x-axis is calculated

$$\sigma_{2j} = t_{2j}^{\infty *}\frac{x}{\sqrt{x^2 - a^2}} + D_s\frac{\Lambda_{j4}}{\Lambda_{44}} \quad j=1,\ 2,\ 3 \tag{42}$$

By using the definition of dynamic intensity factor vector

$$\boldsymbol{K} = [K_{\mathrm{II}}, K_{\mathrm{I}}, K_{\mathrm{III}}, K_D]^T = \lim_{x\to a}\sqrt{2\pi(x-a)}\boldsymbol{t}_2 \tag{43}$$

4 Crack perpendicular to the poling axis, anti-plane problem

In this situation, the infinite plate only subjects to σ_{23}^{∞} and D_2^{∞} . The present authors have studied the anti-plane moving PS model using the continuous distribution dislocation method. In this article, some results will be verified using the complex function method.

From Eq. (**A**.13), we obtain

$$\boldsymbol{K} = [K_{\mathrm{III}}, K_D]^T = \sqrt{\pi a}[\sigma_{23}^{\infty} + \frac{e_{15}}{\varepsilon_{11}}D_2^{\infty}, 0]^T \tag{44}$$

where K_{III} is independent of the crack propagation velocity.

From Eqs. (15), (16) and (A.13), we have

$$\begin{aligned}\sigma_{23} &= \sqrt{\frac{a}{2r}}\Re\left[(\sigma_{23}^{\infty}+\frac{e_{15}}{\varepsilon_{11}}D_2^{\infty})(\cos\theta+\mu_1\sin\theta)^{-\frac{1}{2}}\right] \\ &= \sqrt{\frac{a}{2r}}(\sigma_{23}^{\infty}+\frac{e_{15}}{\varepsilon_{11}}D_2^{\infty})\cos\frac{\theta}{2}\end{aligned} \tag{45}$$

If the ferroelectric material is such that a crack propagates in a direction the maximum shear stress, it can be seen that the maximum shear stress σ_{23} occurs at $\theta=0$ for all the crack speeds. It means the crack remains in its straight line path for all the crack speeds.

5 Conclusions

The transient response of a anti-plane Yoffe-type crack moving with constant velocity in ferroelectric materials is investigated in this paper. The dynamic intensity factors of stress, electric displacement are obtained in explicit forms. When the velocity of the crack $v\to 0$, the moving PS model will reduce to the static PS model. When the size of the electric saturation zone $r\to 0$, the moving PS model is in agreement with the moving linear piezoelectric model. For the case of anti-plane problem, it is concluded that the crack remains in its straight line path for all the crack speeds.

Acknowledgements

The authors are grateful for the support by National Natural Science Foundation of China under Grants #11090330, #11090331, #11072003 and #G2010CB832701.

Appendix

The matrices ***Q***, ***R*** and ***T*** are

$$\boldsymbol{Q}=\begin{bmatrix}c_{44} & e_{15}\\ e_{15} & -\varepsilon_{11}\end{bmatrix},\ \boldsymbol{R}=\begin{bmatrix}0 & 0\\ 0 & 0\end{bmatrix},\quad \boldsymbol{T}=\begin{bmatrix}c_{44} & e_{15}\\ e_{15} & -\varepsilon_{11}\end{bmatrix} \tag{A.1}$$

The eigenproblem given by Eq. (12) becomes

$$\begin{bmatrix}c_{44}-\rho v^2+c_{44}\mu^2 & e_{15}(1+\mu^2)\\ e_{15}(1+\mu^2) & -\varepsilon_{11}(1+\mu^2)\end{bmatrix}\begin{bmatrix}a_1\\ a_2\end{bmatrix}=0 \tag{A.2}$$

Similar to the static case, two characteristic roots are μ_1=i, . μ_2=i β.
in which

$$\beta=(1-v^2/c^2)^{1/2} \tag{A.3}$$

where $c=(\bar{c}_{44}/\rho)^{1/2}$ is the speed of the piezoelectric stiffened bulk shear wave, $\bar{c}_{44}=c_{44}+e^2{}_{15}/\varepsilon_{11}$ is the piezoelectric stiffened elastic constant.

The matrix ***H*** is then

$$\boldsymbol{H}=\frac{2}{\bar{\beta c}_{44}\varepsilon_{11}}\begin{bmatrix}\varepsilon_{11} & e_{15}\\ e_{15} & \dfrac{e_{15}^2}{\varepsilon_{11}}-\bar{\beta c}_{44}\end{bmatrix},\qquad \boldsymbol{\Lambda}=\boldsymbol{H}^{-1}=\frac{1}{2}\begin{bmatrix}\bar{\beta c}_{44}-\dfrac{e_{15}^2}{\varepsilon_{11}} & e_{15}\\ e_{15} & -\varepsilon_{11}\end{bmatrix} \tag{A.4}$$

As $\beta\to 1$ i.e. v=0, $\boldsymbol{H}$ will reduce to the static value [12].

References

[1] Kuna, M., Fracture mechanics of piezoelectric materials—Where are we right now? Eng. Fract. Mech. 77 (2010) 309–326.
[2] Freund, L.B.. Dynamic fracture mechanics. Cambridge: Cambridge Press, 1990.
[3] Chen, Z.T., Yu, S.W., Anti-plane Yoffe crack problem in piezoelectric materials. Int. J. Fracture. 84 (1997) L41-L45.
[4] Soh, A.K., Liu, J.X., Lee, K.L., Fang D.N., On a moving Griffith crack in anisotropic piezoelectric solids. Arch. Appl. Mech. 72 (2002) 458–469.
[5] Li, S., Mataga, P.A., Dynamic crack propagation in piezoelectric materials-part I. Electrode solution. J. Mech. Phys. Solids. 44 (1996a) 1799–1830.
[6] Li, S., Mataga, P.A., Dynamic crack propagation in piezoelectric materials-part II. Vacuum solution. J. Mech. Phys. Solids 44 (1996b) 1831–1866.
[7] To, A.C., Li, S., Glaser, S.D., Propagation of a mode-III interfacial conductive crack along a conductive interface between two piezoelectric materials. Wave Motion. 43 (2006) 368–386.
[8] Chen, X.H., Ma, C.C., Ing, Y.S., Tsai, C.H., Dynamic interfacial crack propagation in elastic–piezoelectric bi-materials subjected to uniformly distributed loading. Int. J. Solids. Struct. 45 (2008) 959–997.
[9] Gao, H., Zhang,T.Y. , Tong,P., Local and global energy release rates for an electrically yielded crack in a piezoelectric ceramic. J. Mech. Phys. Solids. 45 (1997) 491–510.
[10] Shen, S.P., Kuang, Z.B., Nishioka, T., Dynamic mode-III interfacial crack in ferroelectric materials. Int.J.Appl. Electrom. 11 (2000) 211–222.
[11] Suo, Z., Kuo C. M., Barnett, D. M., Willis, J. R., Fracture mechanics for piezoelectric ceramics. J .Mech. Phys. Solids. 40 (1992) 739-765.
[12] Wang, T.C., Analysis of strip electric saturation model of crack problem in piezoelectric materials. Int. J. Solids. Struct. 37 (2000) 6031–6049.
[13] Zhang, T.Y., Gao, C.F., Fracture behaviors of piezoelectric materials. Theor. Appl. Fract. Mec. 41 (2004) 339–379.